Heliyon 9 (2023) e20657

Contents lists available at ScienceDirect

Heliyon

journal homepage: www.cell.com/heliyon

Preparation, characterization, and Co-delivery of cisplatin and doxorubicin-loaded liposomes to enhance anticancer Activities

Mahdi Bahrami Parsa [a], Farzaneh Tafvizi [a,*], Vahid Chaleshi [b], Mostafa Ebadi [c]

[a] Department of Biology, Parand Branch, Islamic Azad University, Parand, Iran
[b] Basic and Molecular Epidemiology of Gastrointestinal Disorders Research Center, Research Institute for Gastroenterology and Liver Disease, Shahid Beheshti University of Medical Science, Tehran, Iran
[c] Department of Biology, Damghan Branch, Islamic Azad University, Damghan, Iran

ARTICLE INFO

Keywords:
Apoptosis
Cisplatin
Co-delivery
Doxorubicin
Liposome
A2780 cell line

ABSTRACT

Ovarian cancer stands as a leading cause of cancer-related deaths among women globally. This malignancy has hindered successful treatment attempts due to its inherent resistance to chemotherapy agents. The utilization of cisplatin and doxorubicin-loaded liposomes emerges as a strategically advantageous approach in the realm of biomedical applications. This strategy holds promise for augmenting drug efficacy, mitigating toxicity, refining pharmacokinetics, and facilitating versatile drug delivery while accommodating combination therapies. In pursuit of scholarly investigations, the eminent databases, including PubMed/MEDLINE, ScienceDirect, Scopus, and Google Scholar, were meticulously scrutinized. Within this study, a nano-liposomal formulation was meticulously designed to serve as a co-delivery system. This system was optimized by varying lipid concentrations, hydration time, and DSPC: cholesterol molar ratios to efficiently encapsulate and load doxorubicin (DOX) and cisplatin (CIS) to overcome drug resistance problems. The Lipo (CIS + DOX) formulation underwent rigorous characterization including dimensions, entrapment efficiencies and drug release kinetics. Notably, the entrapment efficiency of cisplatin and doxorubicin loaded liposomal nanoparticles was an impressive 85.29 ± 1.45 % and 73.62 ± 1.70 %, respectively. Furthermore, Lipo (CIS + DOX) drug release kinetics exhibited pH-dependent properties, with lower drug release rates at physiological pH (7.4) than acidic (pH 5.4). Subsequent cytotoxicity assays revealed the enhanced biocompatibility of dual-drug liposomes with HFF cells compared to free drug combinations. Impressively, CIS and DOX-loaded liposomes induced significant cytotoxicity against A2780 in comparison to free drugs and combinatorial free drugs. Furthermore, the CIS and DOX-loaded liposome showed induced apoptotic potential and cell cycle arrest in A2780 compared to CIS, DOX, and their combination (CIS + DOX). Combining CIS and DOX via liposomal nanoparticles introduces a promising therapeutic avenue for addressing ovarian cancer. These nano-scale carriers hold the potential for attenuating the untoward effects of singular drugs and their attendant toxicities.

* Corresponding author.
E-mail addresses: mahdi_4_bahrami@yahoo.com (M. Bahrami Parsa), Farzaneh.Tafvizi@iau.ac.ir, farzanehtafvizi54@gmail.com (F. Tafvizi), chaleshi@gmail.com (V. Chaleshi), mtf.ebadi@gmail.com (M. Ebadi).

https://doi.org/10.1016/j.heliyon.2023.e20657
Received 25 April 2023; Received in revised form 25 September 2023; Accepted 3 October 2023
Available online 5 October 2023

1. Introduction

Ovarian cancer stands as one of the primary causes of gynecological cancer-associated mortality. Epithelial ovarian cancer commonly receives diagnosis at an advanced stage. Given its extensive metastasis within the abdominal region, it is the fifth most prevalent malignancy in women over 40, trailing only breast cancer [1,2]. A range of treatment strategies presently exists to combat ovarian cancer, encompassing surgical interventions, chemotherapy, and radiation therapy. The selection of the appropriate approach depends on the treatment stages and the overall behavior of cancerous cells [3–5]. Among these strategies, chemotherapy is a prominent and noteworthy option compared to alternative treatments. Cancer chemotherapeutic agents can target cancer cells, inhibiting their growth, division, and further proliferation. Nevertheless, challenges such as adverse effects experienced by patients and the emergence of drug resistance within tumors have constrained the efficacy of chemotherapy [6–8].

Typically, patients are administered either a single drug or a combination of multiple drugs. However, research has demonstrated that combination chemotherapy, involving the simultaneous administration of several drugs, frequently leads to enhanced survival rates among cancer patients when compared to the utilization of single drugs. Consequently, the synergistic effects of multiple drugs have the potential not only to impede tumor growth through the regulation of diverse signaling pathways but also to mitigate the development of multidrug resistance (MDR) [9,10].

Cisplatin, an inorganic molecule, is recognized as a widely used and potent agent. It acts by inhibiting cellular transcription and replication by forming DNA adducts. Cisplatin finds application in the treatment of various solid tumors, including those affecting the breast, ovaries, bladder, throat and lung [11–13]. On the other hand, doxorubicin (DOX), an anthracycline antibiotic, has potent antineoplastic properties. It is used in a wide range of malignancies including breast, thyroid, lung, ovarian, bladder, non-Hodgkin's lymphoma and acute lymphoblastic leukemia. Doxorubicin has the potential to inhibit tumor cell growth by inhibiting DNA intercalation and macromolecular biosynthesis in tumor cells [14,15].

Nevertheless, cisplatin presents several limitations, including bone marrow suppression, nephrotoxicity, and gastrointestinal reactions [16]. Furthermore, the retention period within the body poses a central predicament for cancer drugs. Additionally, the hydrophobic nature of these drugs leads to hepatic elimination, reduced absorption, and low serum bioavailability. Pioneering the application of nanoparticles [17], microspheres [18], liposomes [19], and micelles [20] as drug delivery systems for both CIS and DOX addresses these issues. These advancements mitigate side effects while enhancing safety, efficiency, tolerability, pharmacokinetics, biodistribution, solubility, stability, controllable release, and targeted drug delivery [21,22].

Based on research involving these drugs, optimal results are attained by implementing vesicular systems, particularly liposomes and niosomes, as novel therapeutic methodologies. These niosomal and liposomal nano-carriers enable the sustained and controlled release of encapsulated cargo at the intended site. Furthermore, they facilitate targeted drug delivery, eradicating tumorous cells with minimal systemic toxicity systemic toxicity [23,24].

Liposomes, small spherical vesicles composed of cholesterol and non-toxic natural phospholipids, serve as artificial carriers. From 0.05 to 5.0 μm in diameter, liposomes are classified as micro-particulate or colloidal carriers [25,26]. The efficacy of liposomes as drug delivery systems is derived from their biocompatible and biodegradable nature, characterized by one or more phospholipid bilayers. These vesicles can transport aqueous or lipid-based drugs through their phospholipid bilayer membranes, with the transport mechanism varying depending on the type of drug incorporated. Owing to their favorable attributes such as biocompatibility, biodegradability, low toxicity, and the capacity to encapsulate hydrophilic and lipophilic drugs, research endeavors have been dedicated to utilizing liposomal nano-carriers as a means to mitigate drug toxicity and/or target specific cells [27–29].

The realm of widely utilized chemotherapy medications unquestionably encompasses anthracyclines and platinum-based compounds [30]. Several *in vitro* and in vivo investigations have also explored the coadministration of DOX and CIS to elucidate an augmentation in pharmacological activity owing to synergism while contrasting the effects of these medications when taken individually [31–35].

Both DOX and CIS carry side effects that curtail their usage. However, encapsulating these drugs within liposomes can mitigate their toxicity and minimize associated side effects. This capability is achievable because liposomes can impede the circulation of drugs in the bloodstream and their intrusion into healthy cells, thereby decreasing toxicity and increasing efficacy. Through liposomal encapsulation, it becomes possible to modulate the pharmacokinetics of these drugs to enhance their therapeutic effectiveness. These strategies extend circulation longevity, enhance accumulation in targeted tissues, and regulate drug release for sustained delivery. Cisplatin and Doxorubicin can be synergistically combined with other drugs or therapies within liposomes to amplify their efficacy further and overcome drug resistance [36,37]. Moreover, liposomes can be equipped with ligands, targeting agents, or imaging agents to enhance drug precision and delivery. Alongside these benefits, liposomal co-delivery technology has effectively eradicated invasive cancer cells and associated vasculogenic mimicking channels [38–41]. Numerous investigations into the anticancer efficacy of co-delivering CIS and DOX through liposomal formulation have been conducted *in vitro* and animal models. However, to our knowledge, there is a dearth of data concerning the optimization and anticancer activity of these nanocarriers against the A2780 ovarian cancer cell line. The pivotal innovation of the present study lies in optimizing the nanoliposome formulation to augment cellular toxicity, induce apoptosis, curtail cellular necrosis and drug resistance, and enhance the effectiveness of the drug combination for ovarian cancer therapy. Hence, this contemporary investigation tailored liposomal nano-carriers that concurrently co-deliver CIS and DOX *chemotherapeutic* agents for ovarian cancer treatment.

Therefore, in the current study, liposomal nanocarriers were designed for the precise simultaneous co-delivery of both CIS and DOX chemotherapeutic drugs for the treatment of ovarian cancer. For this purpose, the potency of nanoliposomes loaded with CIS and DOX [Lipo (CIS + DOX)] was prepared, then characterization and *in vitro* environments were evaluated. The effects of variable lipid content, DSPC: cholesterol molar ratio and hydration time were analyzed in terms of particle size, entrapment efficiency and polydispersity

index (PDI). The *in vitro* release behavior was studied at different pHs. The therapeutic effects of Lipo (CIS + DOX) were further investigated in terms of cytotoxicity of the nanoformulations against cancer and normal cell lines. Further analyses, including flow cytometry and cell cycle arrest, were also investigated to evaluate the cell apoptosis rate and growth inhibitory effect of the combined drug-loaded liposomes. For conducting this study, the most reputable databases—PubMed/MEDLINE, ScienceDirect, Scopus, and Google Scholar—were meticulously scoured to ascertain pertinent literature. The research was executed during the timeframe spanning 2020 to 2022.

2. Materials and methods

2.1. Materials

Doxorubicin (DOX) and cisplatin (CIS) were procured from Millipore Sigma (Burlington, MA, USA) and utilized without subsequent purification. Cholesterol and distearoylphos phatidyl choline (DSPC) were also obtained from Millipore Sigma. Chloroform, methanol, phosphate-buffered saline (PBS), sodium dodecyl sulfate (SDS), dialysis membrane (MWCO 12,000 Da), dimethyl sulfoxide (DMSO), and Amicon (Ultra-15 Membrane, MWCO 30,000 Da) were sourced from Merck Chemical Co. (Darmstadt, Germany).

The HFF and A2780 cell lines were sourced from the Pasteur Institute Cell Bank (Tehran, Iran). Trypan blue, trypsin-EDTA, formaldehyde, fetal bovine serum (FBS), phosphate buffer, 100X penicillin/streptomycin (PS), RPMI-1640 medium (Dulbecco's Modified Eagle Medium), and 3-(4,5-dimethylthiazol-2-yl)-2,5-diphenyltetrazolium bromide (MTT) were acquired from Gibco, ThermoFisher Scientific (Waltham, MA, USA). The Annexin V-FITC flow cytometry kit and 1X binding buffer were procured from Affymetrix Biosciences, ThermoFisher Scientific.

2.2. Optimization of liposomal formulations

The optimization of the liposomal formulation comprising both CIS and DOX (referred to as Lipo (CIS + DOX)) was conducted using a central composite design (CCD) approach (Design Expert, Version 11, Stat-Ease Inc. Minneapolis, USA). This method involved manipulating three factors, each with three distinct levels. The independent variables employed in this study are outlined in Table 1, accompanied by their corresponding levels: low, medium, and high. These levels were systematically varied to gauge the impact on three critical responses: encapsulation efficiency, size, and the formulation's Polydispersity Index (PDI).

The Design-Expert software (Version 13, Stat-Ease, Inc., Minneapolis, MN, USA) was employed to establish a polynomial equation that accurately represented the experimental conditions and outcomes. After optimization, the data derived from the optimal design configuration were meticulously analyzed. The process entailed a meticulous comparison between the experimental data and the predicted responses, ultimately selecting the formulation with the highest degree of optimization for further investigation using the point prediction method.

2.3. Synthesis of liposomal formulations

Liposomes were generated utilizing the thin-film hydration technique [42]. Accurate measurements of cholesterol and surfactant were weighed and dissolved in 9 mL of chloroform/methanol (2:1; v/v) within a round-bottom flask. The organic solvent was gradually evaporated at 60 °C and 150 rpm for 30 min under reduced pressure using a rotary flask evaporator, forming a thin dried film on the interior surface of the round-bottom flask. This thin film was desiccated through continuous flask rotation, with residual solvents eliminated under vacuum conditions overnight.

For the hydration of the desiccated lipid film, 10 mg of PBS (pH 7.4) containing CIS and DOX was employed. After hydrating the lipid film with the mentioned reactants, the specimens were desiccated at 60 °C and 150 rpm for 30 min to achieve dry samples. Following this step, the homogenized samples were achieved using an ultrasonic processor (UP50H compact laboratory homogenizer, Hielscher Ultrasonics, Teltow, Germany), ensuring the optimal size distribution of Lipo (CIS + DOX).

2.4. Physical characterization of liposomal formulations and morphology

The vesicle size and size distribution of the Lipo (CIS + DOX) formulations were determined through benchtop dynamic light scattering (DLS) employing Malvern Panalytical Ltd., (Malvern, United Kingdom). Prepared samples were diluted in deionized water to minimize complex scattering effects. Subsequently, the shape and surface characteristics of the liposomal formulation of Lipo (CIS + DOX) were observed using both Field Emission Scanning Electron Microscopy (FE-SEM) and Transmission Electron Microscopy (TEM).

Table 1
Different levels for variables in the Box–Behnken design optimization.

Level	−1	0	+1
A (Lipid, μmoL)	200	250	300
B (Hydration time, min)	30	45	60
C (DSPC: Cholesterol, molar ratio)	75:25	50:50	25:75

Drug concentration: 1 mg/mL, Sonication time:5 min.

For imaging purposes, FE-SEM was conducted using the NOVA NANOSEM 450 FEI model, operating at an accelerating voltage of 15 kV. During TEM analysis, a drop of Lipo (CIS + DOX) was placed on a carbon-coated copper film and stained with 1 % phosphotungstic acid. The imaging was carried out at 100 kV using the Zeiss EM900 Transmission Electron Microscope in Jena, Germany.

2.5. Fourier-Transform Infrared Spectroscopy (FT-IR)

Utilizing Fourier-Transform Infrared Spectroscopy (FT-IR) with the Spectrum Two instrument in Waltham, MA, USA, to determine whether CIS and DOX were physically or chemically loaded into the nanoparticles, polymer samples were blended with KBr. The resulting mixture was compressed under hydraulic strain to form pellets, and spectral readings were taken within the 400–4000 cm^{-1} wavelength range.

2.6. Differential Scanning Calorimetry analysis (DSC)

Thermal properties were evaluated using Differential Scanning Calorimetry (DSC) through the Netherlands PerkinElmer PYRIS 6 DSC INTRACOOLER instrument. The free drugs (CIS and DOX), liposomes, and CIS + DOX-loaded liposomes were dried using the alpha 1–2 ld plus freeze dryer manufactured by Martin Christ GmbH, Germany. Before DSC analysis, the free CIS, DOX, and the liposomal formulations of the dual drugs were freeze-dried. Approximately 5 mg of the samples were precisely weighed and sealed within aluminum pans. These pans were maintained at an isothermal condition of 20 °C for 30 min. The liposomal formulations were examined under a nitrogen atmosphere, employing a heating range from 30 °C to 300 °C, with a scanning rate of 10 °C/min. The baseline was established using a blank aluminum pan as a reference.

2.7. Entrapment efficacy

The liposomal formulations underwent ultra-filtration utilizing the Eppendorf® 580R centrifuge in Hamburg, Germany. The Amicon Ultra-15 membrane was used for this purpose, and the centrifugation was carried out at 4000 rpm for 20 min at a temperature of 4 °C. This process facilitated the separation of drug-carrying liposomes from unencapsulated drugs, enabling the assessment of the percentage entrapment efficacy (EE%). The concentrations of free drugs were determined spectrophotometrically, with measurements taken at 480 nm for DOX and 510 nm for CIS, using the UV–visible light spectrophotometer model UV-1700 PharmaSpec manufactured by Shimadzu in Kyoto, Japan. The calculation of entrapment efficacy (%) was accomplished using Equation (1):

$$\text{Entrapment Efficacy}\% = [(A - B) / A] \times 100 \quad (1)$$

where (A) signifies the initial CIS or DOX concentration during liposomal preparation, and (B) represents the concentration of non-entrapped CIS or DOX after centrifugation.

2.8. In vitro drug release and the release kinetics

2.8.1. Evaluation of drug release and release kinetics

In order to conduct a comparative assessment of drug release among the various samples, we placed 2 mL of free drug and Lipo (CIS + DOX) within a semipermeable acetate cellulose dialysis bag (MWCO 12 kDa). Subsequently, we submerged this bag in a 50 mL PBS solution (pH 5.4, 7.4, 1X concentration). The experimental setup underwent gradual agitation at 37 °C with a rotational speed of 50 rpm over 72 h. At designated time intervals, we extracted 1 mL of the release medium and replaced it with an equal volume of fresh PBS-SDS. We then subjected the withdrawn samples to analysis at 480 nm and 510 nm, with the corresponding concentrations determined using an ultraviolet light spectrophotometer. We utilized the free drug as a control group throughout the experiment and replicated this procedure accordingly. Notably, the drug concentration remained consistent inside and outside the dialysis bag.

Firstly, the CIS, DOX, and CIS + DOX release kinetics from the samples were examined utilizing established mathematical models. These models encompass the zero-order model (Equation (2)) (cumulative % drug release vs. time), first-order model (cumulative % drug remaining vs. time) (Equation (3)), Higuchi model (cumulative % drug release vs. square root of time) (Equation (4)), and Korsmeyer-Peppa model (log cumulative % drug release vs. log time) (Equation (5)) [43].

Equation (2): Zero-order Model

$$C_t = C_0 + K_0 t \quad (h^{-1}) \quad (2)$$

In this Equation, C_t represents the quantity of drug dissolved at time t, C_0 symbolizes the initial amount of drug within the solution, and K_0 signifies the constant for zero-order release.

Equation (3): First-order Model

$$\text{Log } C = \text{Log } C_0 - Kt / 2 \cdot 303 \quad (h^{-1}) \quad (3)$$

Equation (3) captures the first-order release kinetics, with C_0 representing the initial drug concentration, K denoting the first-order release constant, and t signifying time.

Equation (4): Higuchi Model

$$Q = K_H\sqrt{t} \quad (4)$$

The Higuchi model, as depicted in Equation (4), correlates the amount of drug released over time t per unit area. Q is the released drug quantity, and K_H is the Higuchi dissolution constant.

Equation (5): Korsmeyer-Peppas Model

$$M_t/M_\infty = Kt^n \quad (5)$$

The Korsmeyer-Peppas model, represented by Equation (5), establishes a relationship between the fraction of drug released (M_t/M_∞) at time t, the release rate constant (K), and the release exponent (n). The value of the exponent (n) provides insights into the mechanism governing drug release.

2.9. Stability study

A stability study was conducted on the optimized formulations at temperatures of 25 ± 1 °C or 4 ± 1 °C, with a relative humidity of 60 ± 5 % over one month. The formulation stability investigation measured the optimum formula's average encapsulation efficiency (EE%), particle size, and polydispersity index (PDI).

2.10. Culture of A2780 and HFF cell lines

The A2780 and HFF cell lines were cultured at 37 °C under atmospheric conditions containing 5 % CO_2. RPMI-1640 fresh medium supplemented with 10 % fetal bovine serum (FBS), 100 U/mL penicillin, and 100 U/mL streptomycin (comprising the complete growth medium) was utilized for maintaining the HFF and A2780 cell lines. Upon reaching 80 % confluency, the medium was aspirated, cells were trypsinized using 0.25 % (w/v) trypsin-EDTA, and subsequent culturing was carried out. Before each experiment, the enumeration of cell number and viability assessment was performed through the trypan blue dye exclusion test.

2.11. Cell cytotoxicity

The viability assessment of A2780 ovarian cancer cells and normal fibroblast cells (HFF) was conducted using the MTT assay. Cells were cultured for one and two days in the presence of varying concentrations of Lipo (CIS + DOX), free CIS, free DOX, CIS + DOX, and unloaded liposomes (Lipo) (ranging from 1.56 to 100 μg/mL). For the A2780 cancer cells, which were seeded into 96-well plates (10^4 cells/well), cell incubation was carried out for 24 and 48 h. Similarly, HFF cells were exposed to concentrations of the mentioned formulations and incubated for 24 h to evaluate their toxicity. Cell proliferation was determined using 0.5 mg/mL of MTT, which reduced the colorless tetrazolium dye (MTT) to insoluble formazan with a purple color. The ensuing formazan was solubilized in 100 μL of DMSO to quantify cells' oxidoreductase enzymatic activity. The calculation of cell viability percentage was achieved using the following formula:

Cell viability (%) = Optical Density $_{570}$ treatment/Optical Density $_{570}$ control × 100 %

2.12. Analysis of apoptosis

The Annexin V-FITC/PI double staining method was employed to assess the apoptosis of A2780 cells. Apoptosis induction involved the treatment of cancer cells with unloaded liposomes (Lipo), free CIS, free DOX, CIS + DOX, and Lipo (CIS + DOX) during a 48-h incubation period. Initially, cells (1×10^5 cells/well) were subjected to two washes with PBS and then suspended in 1X binding buffer. Subsequently, annexin V-FITC (emitting green fluorescence) and propidium iodide (yielding red fluorescence) were utilized to differentiate apoptotic and normal cells. A benchtop flow cytometer (FACSCalibur, BD Biosciences, Franklin Lakes, NJ, USA) was employed to analyze these samples, which were carried out in triplicate. All experiments were executed using the IC_{50} concentration.

2.13. Cell cycle arrest

Cell proliferation and cell cycle progression were assessed through propidium iodide (PI) staining. Cells (1×10^6 cells/well) were seeded in 6-well plates and incubated overnight. Following treatment with unloaded liposomes (Lipo), free CIS, free DOX, CIS + DOX, and Lipo (CIS + DOX) for 48 h in a complete medium, cells were harvested and fixed overnight at 4 °C using 70 % cold ethanol. Subsequent washing with PBS was carried out, followed by staining with 500 μL of PI solution containing RNase in the dark for 20 min at room temperature. This process was repeated three times, and the analysis was conducted using flow cytometry.

2.14. Statistical analysis

Values are presented as the mean ± standard deviation (SD) and calculated using GraphPad Prism version 8 (GraphPad Software, Inc., San Diego, CA, USA). Differences were assessed using the ANOVA test, and a $P < 0.05$ was deemed statistically significant.

3. Results & discussion

3.1. Characterization of nano-carriers

3.1.1. Particle size

Cisplatin and doxorubicin-loaded liposomes, denoted as Lipo (CIS + DOX), were optimized using a three-factor, three-level Box–Behnken statistical design. Before designing Lipo (CIS + DOX), calibration curves were constructed for each drug separately. Validation of DOX and CIS was established at 480 nm and 510 nm, respectively, displaying linear regression for each sample with correlation coefficients of 0.9977 for DOX and 0.9906 for CIS (Fig. S1). Post-validation, three independent variables were evaluated: lipid concentration, hydration time, and DSPC: cholesterol ratio. Encapsulation efficiency (EE%), particle size, and PDI were chosen as the dependent variables. A comparison was made between the experimental response values and the predicted values generated by the model equations. The data from the regression plot exhibited a linear relationship between actual and predicted response values. Significant coefficients and R^2 values were used to assess the models. Ultimately, an optimal formulation was selected through the point prediction method for further investigation. The outcomes of the Box–Behnken trials are outlined in (Table 2).

The particle size range for Lipo (CIS + DOX) formulations fell between 153.4 nm and 289.9 nm (Table 2). According to Table S1, the best-fitted model for particle size was quadratic and exhibited significance ($P < 0.03$). Lipid concentration and hydration time significantly influenced particle size. However, the P-value for DSPC: cholesterol ratio exceeded 0.05, indicating its negligible impact on particle size. Fig. 1A, B and 1C depict the response surface illustrating the effects of lipid concentration, hydration time, and DSPC: cholesterol ratio on particle size.

The regression equation below elucidates that higher lipid concentration led to the formation of larger vesicles, as shown by the following Equation (Table S2):

Size = +154.37 + 20.45* A −27.36* B −12.96* C +0.025* AB +10.18* AC +16.00* BC +39.74* A2 +19.27* B2 +40.27* C2

One possible explanation is that an increase in lipid amount from 200 to 300 μmoL results in more excellent area coverage by lipid molecules, leading to increased membrane fluidity and observed liposome size growth. Furthermore, higher lipid concentration increases membrane rigidity, which enhances resistance to sonication and leads to the formation of more giant vesicles. In contrast, liposome size decreases with prolonged hydration time. Longer hydration times disrupt the vesicular structure, potentially causing drug leakage and size reduction [44,45]. Additionally, including cholesterol in DSPC (reducing the DSPC: cholesterol ratio from 75/25 to 25/75) amplifies the average vesicle size. This phenomenon can be attributed to the increased hydrophobicity of the lipid bilayer as the hydrophilic head of cholesterol penetrates the bilayer, inducing membrane disorder and increasing vesicle size [46].

3.1.2. Polydispersity index (PDI)

In the model fitting of the Polydispersity Index for liposomes, the sequential P-value of the linear model was estimated to be 0.01. All formulations exhibited PDI values of less than 0.9, indicating a narrow size distribution and excellent homogeneity (Table 2). P-values of PDI for all independent variables, except A, AB, AC, and BC models in Table S3, were below 0.05. As per Table S3, lipid concentration, hydration time, and the DSPC: cholesterol ratio significantly affected the PDI value ($P < 0.05$). The following regression equation describes the relationship between PDI and the independent variables:

PDI = +0.19 + 0.019 *A −0.036 *B −0.028 *C −0.023 *AB +0.015 *AC +2.500E-004 *BC + 0.072 *A2 +0.056 B2 +0.041 * C2

Fig. 1D, E, and 1F depict 3D contour plots illustrating the effects of DSPC: cholesterol ratio, hydration time, and lipid concentration on the PDI value. The data for the regression equation concerning PDI are presented in Table S4. The regression analysis for the PDI responses indicates that lipid concentration positively influences the PDI value. However, hydration time and the DSPC: cholesterol ratio negatively affects the PDI value. The increase in PDI value with higher lipid concentration is the presence of more liquid molecules in liposomes, which reduces the negative charge and enhances the aggregation tendency of nanoparticles [47].

Table 2
Design of experiments using Box–Behnken method to optimize the liposomal formulation of CIS + DOX.

Run	Levels of independent variables			Dependent variables			
	A	B	C	Average size (nm)	PDI	Entrapment Efficiency (EE) (DOX, %)	Entrapment Efficiency (EE)(CIS, %)
1	0	−1	1	203.3	0.294	71.25	66.42
2	−1	0	1	198.7	0.245	77.39	74.37
3	−1	0	−1	216.3	0.348	72.49	68.21
4	0	0	0	153.4	0.192	75.21	76.83
5	1	0	−1	249.7	0.333	73.33	70.94
6	1	1	0	205.4	0.279	75.41	73.82
7	0	0	0	162.5	0.201	76.82	74.49
8	−1	−1	0	221.4	0.312	65.22	63.39
9	1	0	1	272.8	0.289	83.92	77.25
10	0	−1	−1	289.9	0.331	62.42	57.32
11	−1	1	0	177.3	0.263	68.83	70.25
12	0	1	1	169.9	0.246	78.37	76.12
13	0	0	0	147.2	0.178	77.04	75.41
14	0	1	−1	192.5	0.282	61.34	69.32
15	1	−1	0	249.4	0.421	80.36	73.39

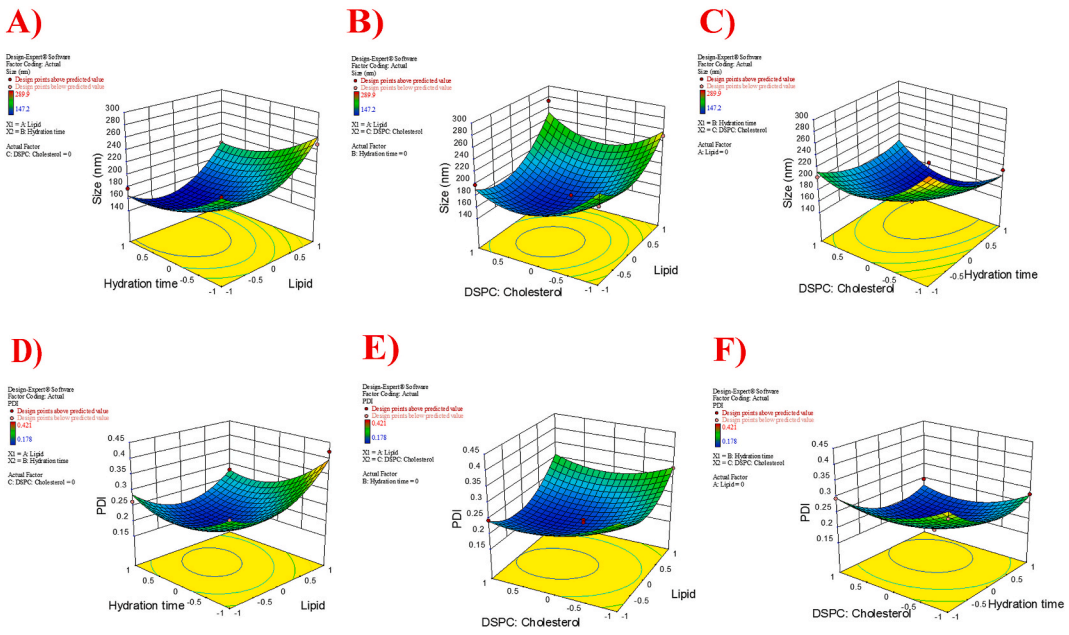

Fig. 1. Box-Behnken method for size (A-B-C) and Polydispersity Index (D-E-F) as a function of the independent parameters.

Although the results of the regression equation demonstrate a linear decline in liposomal polydispersity index values with increasing hydration time, the increase in hydration time can lead to drug leakage from vesicles, resulting in smaller particle sizes, a decrease in PDI and, consequently, a more homogeneous distribution. Additionally, the inverse relationship between PDI and the DSPC: cholesterol ratio may be attributed to differences in lipid tail length, molecular shape, and membrane fluidity [48,49].

3.1.3. Entrapment efficacy (EE%)

Table 2 presents a summary of the EE% of CIS + DOX encapsulated in liposomes. High entrapment efficiency refers to the percentage of the total drug (CIS + DOX) encapsulated within the nano-carriers. The maximum entrapment efficacy achieved for CIS and DOX was 77.25 % and 83.92 %, respectively. Notably, a significant synergistic effect of lipid concentration, hydration time, and the DSPC:cholesterol ratio was observed on the percent encapsulation efficacy of DOX (EE%; $P < 0.05$) (Table S5). Additionally, for CIS,

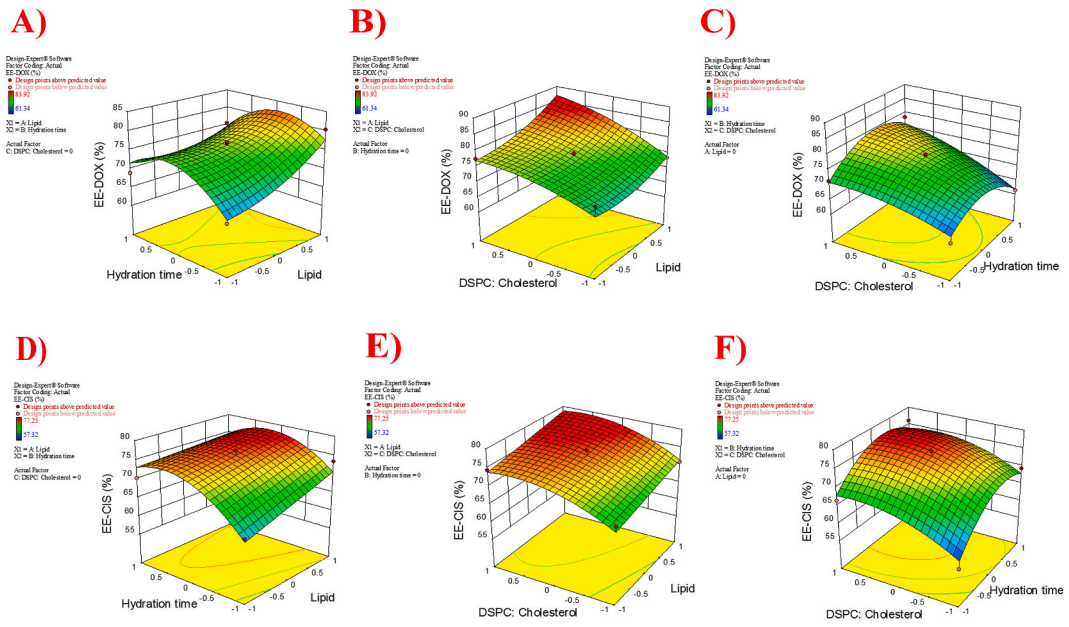

Fig. 2. Box-Behnken method for encapsulation efficiency (EE%) of DOX (A-B-C) and CIS (D-E-F) as a function of the independent parameters.

three independent variables positively influenced entrapment efficacy (Table S6). The regression equations for EE% of DOX and CIS are provided in Tables S7 and S8. The resulting equations, in terms of coded values, are as follows:

$$EE\%\text{-}DOX = +76.36 + 3.64 *A +0.59 * B +5.17 * C -2.14 * AB +1.42 * AC +2.05 * BC +2.27 * A^2 -6.17 * B^2 -1.84 * C^2$$

$$EE\%\text{-}CIS = +75.58 + 2.40 *A +3.62 * B +5.17 * C -2.14 * AB +1.42 * AC +2.05 * BC +2.27 * A^2 -6.17 * B^2 -1.84 * C^2$$

The effects of the DSPC: cholesterol ratio, hydration time, and lipid value on EE% for DOX and CIS drugs, represented as 3D contour plots, are depicted in Fig. 2A, B, and 2C. Furthermore, the effects of the three independent variables on EE% for CIS illustrated as 3D contour plots, are displayed in Fig. 2D, E, and 2F. The observed increase in EE% with extended hydration time can be attributed to the enhanced drug encapsulation within the bilayer and aqueous compartments of the vesicles. The lipid compartment and aqueous phase became saturated with the drug as hydration time increased [50]. Furthermore, elevating the DSPC: cholesterol ratio led to a less permeable liposomal membrane, thereby increasing the percentage of encapsulation efficiency [51].

3.1.4. Validity of the central composite design

Adjusted R^2 demonstrates reasonable concurrence with predicted R^2 when the two values are within 0.20 of each other [52]. Upon examining the data from the regression analysis for various responses presented in Tables S2, S4, S7, and S8, a substantial alignment between R^2 and adjusted R^2 becomes apparent. Additionally, the adequate precision assesses the signal-to-noise ratio. Given that all responses exceed 4, the model can effectively guide the design process.

3.1.5. Data optimization

The optimized Lipo (CIS + DOX) formulation was selected based on achieving a narrow particle size, minimal polydispersity, and a maximal entrapment efficiency percentage. The central composite design technique was employed to predict the optimal formulation. Remarkably, a high desirability index (desirability = 0.802) was attained when the DSPC: cholesterol ratio stood at 60:40, the lipid value was 272.2 μmoL, and the hydration time reached 43.395 min (Table S9). The projected particle size, polydispersity index, and entrapment efficacy of DOX and CIS within the Lipo (CIS + DOX) formulations were 176.66 nm, 0.217, 80.31 %, and 77.25 %, respectively. The resultant formulation was formulated and assessed, and the collected data revealed that the variance between predicted and experimental responses was insignificant, affirming the validity of the optimization process. The values for the optimized formula are outlined in Table 3.

The size of liposomes increased from 129.5 ± 3.96 to 173.8 ± 6.28 nm upon loading with CIS-DOX. This size augmentation can be attributed to the encapsulation of CIS and DOX within the liposomal structure. Moreover, the size increment in liposomes loaded with CIS + DOX, compared to pristine liposomes, can be linked to the more significant amount of enclosed CIS-DOX within the vesicles [52]. The optimized unloaded liposomes exhibited a smaller PDI value (0.168 ± 0.007) compared to the optimized liposomal formulations loaded with CIS-DOX (0.231 ± 0.013), potentially resulting from alterations in vesicle size during the loading process. Furthermore, the EE% of DOX and CIS in the liposomal formulations was 85.29 ± 1.45 % and 73.62 ± 1.70 %, respectively. This discrepancy in EE% suggests that DOX achieves superior loading in liposome structures via electrostatic interactions and the formation of amide and hydrogen bonds compared to CIS [53].

The zeta potential of liposomes containing CIS, DOX, and pristine liposomes is presented in Table 3. Following the loading of liposomes with CIS + DOX, the zeta potential decreased from −28.7 ± 1.25 mV to −22.9 ± 1.53 mV. These repulsive forces play a crucial role in maintaining the colloidal stability of nanoparticles that bear positive or negative charges within low ionic strength aqueous solutions [54]. Considering the positive charge of cisplatin, CIS + DOX-loaded liposomal nanoparticles exhibited a more positive zeta potential in contrast to pristine liposomes [55].

3.2. Size distribution and morphology of the nano-formulations

The morphology and size of nanoparticles are critical parameters in liposomal drug delivery. Small nanoparticles exhibit higher cellular uptake and transfection efficiency than larger ones, facilitating the targeted delivery of particles to specific cells for pharmaceutical functionality [56]. The structure and surface morphology of Lipo (CIS + DOX) were investigated using scanning electron microscopy (SEM) and transmission electron microscopy (TEM). The FE-SEM images of the optimized Lipo (CIS + DOX) formulation are presented in Fig. 3A, revealing that Lipo (CIS + DOX) exhibits a uniform globular morphology with a smooth surface. The particle

Table 3
The optimized responses obtained by Box–Behnken method and the experimental data for the same responses under the optimum conditions, CIS + DOX.

Parameter	Predicted by Box–Behnken method	Lipo (CIS + DOX)	unloaded liposome (Lipo)
Average size (nm)	176.661	173.8 ± 6.28	129.5 ± 3.96
PDI[a]	0.217	0.231 ± 0.013	0.168 ± 0.007
EE%[b] **(DOX)**	80.313	85.29 ± 1.45	–
EE%[b] **(CIS)**	77.250	73.62 ± 1.70	–
Zeta Potential (mV)	–	−22.9 ± 1.53	−28.7 ± 1.25

[a] Polydispersity Index.
[b] Entrapment Efficiency%.

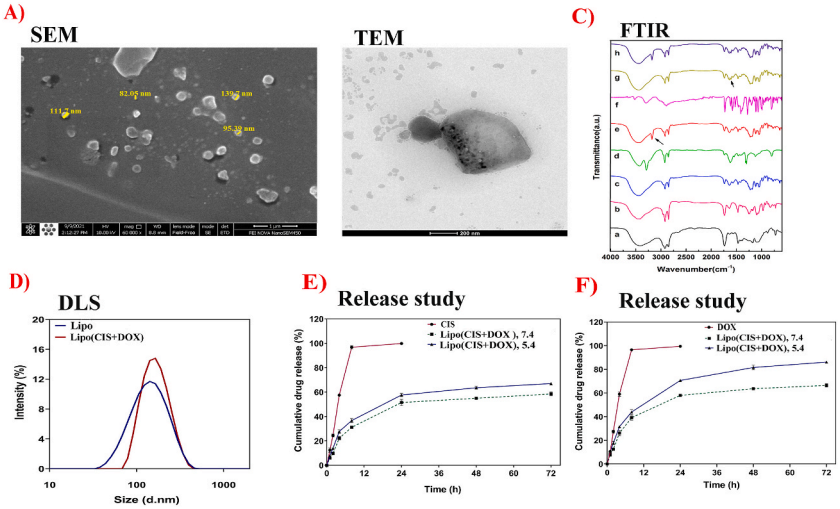

Fig. 3. (A) FE-SEM and (B) TEM photograph of cisplatin and doxorubicin-loaded liposomes [Lipo (CIS + DOX)], (C) FT-IR spectra of a: Cholesterol, b: DSCP, c: Liposome, d: Cisplatin, e: Cisplatin loaded liposomes, f: Doxorubicin, g: Doxorubicin-loaded liposomes, h: Lipo (CIS + DOX), (D) DLS analysis of Lipo (CIS + DOX), (E) *In vitro* release of free CIS, Lipo (CIS + DOX) at pH 7.4, and Lipo (CIS + DOX) at pH 5.4. (F) *In vitro* release of free DOX, Lipo (CIS + DOX) at pH 7.4, and Lipo (CIS + DOX) at pH 5.4.

size was below 300 nm, enabling efficient cellular entry. The results from TEM confirmed the formation of solid, spherical, monodispersed CIS-DOX-loaded liposomal nanoparticles (Fig. 3B). For the determination of size distribution, dynamic light scattering (DLS) analysis was conducted using a particle size analyzer, comparing the size distribution of unloaded liposomes and Lipo (CIS + DOX) nanoparticles (Fig. 3D). Notably, DLS assesses nanoparticle size based on hydrated vesicles, while TEM analyzes nanoparticle size in a dehydrated state (measuring the precise diameter of each particle). It is important to note that, due to the absence of water in dried vesicles despite water being present in the diluted dispersion, the vesicle size measured via TEM is smaller than that from DLS [57].

3.3. Analysis of Fourier Transform Infrared (FT-IR)

Samples including DSPC, cholesterol, unloaded liposomes, free DOX and CIS, DOX-loaded liposomes (Lipo-DOX), CIS-loaded liposomes (Lipo-CIS), and DOX–CIS–loaded liposomes [Lipo (CIS + DOX)] were subjected to characterization using FT-IR spectrophotometry (Fig. 3C). Changes influence the biological activity of therapeutic compounds in their chemical structures. The FT-IR spectrum of the cholesterol formulation (Fig. 3C–a) reveals peaks in the range of 1036–1389 cm^{-1}, indicative of the C–H_2 bending band, while the C–C stretching aromatic peak appears at 1517 cm^{-1}. Furthermore, peaks at 1674 and 1728 cm^{-1} are attributed to C═C and C═O stretching in cholesterol. The FT-IR spectrum of DSPC (Fig. 3C–b) shows peaks related to P–O at 722 cm^{-1} and 826 cm^{-1} frequencies, P═O stretching at 1243 cm^{-1}, and a broadband representing C–N in the range of 1000–1350 cm^{-1}. The characteristic peaks of blank liposomes (Fig. 3C–c) are observed at 1045 cm^{-1} due to P═O symmetric, 1214 cm^{-1} due to P═O symmetric stretching vibration, 1749 cm^{-1} due to C═O group, and 1645 cm^{-1} and 3478 cm^{-1} due to O–H bending and stretching, respectively.

In its pure form, DOX exhibits characteristic band peaks at 1630 cm^{-1} due to the C═O group, 1723 cm^{-1} due to the carboxylic acid group, and 3518 cm^{-1} due to N–H stretching (Fig. 3C–f). The FT-IR pattern for Lipo-DOX (Fig. 3C–g) peaks at 3284 cm^{-1}, indicating DOX's successful incorporation into liposomes.

Fig. 3C–g demonstrates that all characteristic liposome peaks have shifted to different wavenumbers, signifying intermolecular forces between Doxorubicin and liposomes. Additionally, the C═O stretching of DOX appears at a lower wavelength (1604 cm^{-1}), affirming the successful encapsulation of DOX in liposomes. The FT-IR spectrum of Lipo-CIS exhibits peaks at 3187 cm^{-1}, confirming the presence of N–H stretching in Cisplatin and validating its encapsulation within liposomes (Fig. 3C–e). Finally, the FT-IR spectra of the Lipo (CIS + DOX) formulation (Fig. 3C–h) demonstrate that the shifts in characteristic peaks of unloaded liposomes, DOX, and CIS indicate the successful encapsulation of both DOX and CIS drugs within the liposome formulation.

3.4. Drug release and modeling kinetic

The drug release profiles of pure CIS and pure DOX were examined under physiological pH (7.4) and cancerous pH (~5.4) conditions in phosphate-buffered saline-sodium dodecyl sulfate for 72 h (Fig. 3E and F). Generally, an initial burst release of CIS occurred from both pure CIS and CIS + DOX liposomal formulations within the initial 12 h under physiological pH (7.4). The initial burst release of pure CIS at pH 7.4 reached nearly 100 % after 12 h. However, the release of CIS from the liposomal formulation was approximately 50 % (Fig. 3E). Similar outcomes were also observed for DOX (Fig. 3F).

CIS and DOX release rates from liposomal nanoparticles at physiological pH were significantly lower than those of formulations at cancerous pH. Specifically, DOX release rates were 58.01 % and 70.65 %, while CIS release rates were 51.55 % and 57.67 % after 24 h.

This behavior can be attributed to the distinct response of liposomes under different conditions. Liposome nanoparticles tend to swell and rupture in acidic environments but effectively retain drugs under physiological conditions. Furthermore, electrostatic interactions between the drug and the surfactant and the ionization state at physiological pH lead to reduced release at pH 7.4 [58,59]. The release rates of CIS from Lipo (CIS + DOX) under physiological pH were lower than those of DOX from Lipo (CIS + DOX), resulting in cumulative releases of 58.52 % (CIS) and 66.47 % (DOX) over 72 h. The interactions between the drugs and liposomal nanoparticles can explain this discrepancy. DOX molecules can become entrapped between the liposome chains through hydrogen bonding and terminal attachment. In contrast, CIS primarily entraps liposomes through terminal attachment [60].

The release kinetics of pure CIS, DOX, and Lipo (CIS + DOX) formulations at various pH levels were assessed using different kinetic models (Table 4). The selection of the most suitable model for each formulation was determined based on the highest R^2 value, reflecting the goodness of fit. The data in Table 4 shows that the first-order model best fits pure DOX and pure CIS. However, the optimized Lipo-(DOX + CIS) formulation at pH 7.4 and 5.4 adheres to the Korsmeyer-Peppas model. The obtained n values in the Korsmeyer-Peppas kinetic model for all samples ranged from 0.43 to 0.85, indicating the presence of an anomalous transport mechanism governing the release of DOX and CIS molecules from the prepared formulations.

3.5. Differential Scanning Calorimetry

DSC analyses were performed on the unloaded liposome, DOX, CIS, and Lipo (CIS + DOX) formulations. The liposome, consisting of phospholipids and cholesterol, exhibited a slight broad exothermic peak at 47 °C and additional minor exothermic peaks spanning from 90 °C to 110 °C. These features suggest interactions between lipid components during the formation of phospholipids (Fig. 4A). In the DSC traces, DOX displayed a melting endotherm at 196.85 °C, accompanied by exothermic peaks at 208.89 °C, 227.68 °C, and 254.92 °C (Fig. 4B). The appearance of an endothermic peak at 49.62 °C in the thermogram of pure CIS and the physical mixture indicated drug melting (Fig. 4C).

Upon concurrent loading of CIS and DOX drugs into liposomes, the characteristic endothermic peaks of liposomes and drugs shifted to higher temperatures. This shift confirms the existence of hydrogen bonding between the –OH group in liposomes and drugs, resulting in enhanced stability and rigidity of the niosome structure [61] (Fig. 4D). Upon drug incorporation into liposomes, the characteristic endothermic peaks of DOX at 196.85 °C and CIS at 49.62 °C disappeared, indicating the presence of drugs in a molecular dispersion state within the polymeric system. The absence of distinct CIS and DOX peaks in liposomes suggests that the drugs within the liposomes adopted an amorphous state.

3.6. Stability

The investigation into the physical stability of Lipo (CIS + DOX) formulations encompassed two distinct temperatures—25 °C, denoting room temperature, and 4 °C, representing refrigerator storage conditions. This inquiry spanned 60 days, during which the samples' size, polydispersity index, and encapsulation efficiency were meticulously evaluated (Fig. 5A, B, and 5C).

Fig. 5A, B and 5C underscore that the Lipo-(DOX + CIS) compositions stored at 4 °C for up to 30 days exhibited negligible size and encapsulation efficiency alterations. This phenomenon can be attributed to the heightened stability exhibited by hydrophobic liposomes at lower temperatures, juxtaposed with the tendency of liposomal formulations to swell and rupture when stored at elevated temperatures. Consequently, the storage condition engenders a conspicuous expansion in liposome size and polydispersity index (PDI), concomitant with a reduction in encapsulation efficiency [62].

An evaluation of vesicle size for drug-loaded liposomes conducted at 25 °C revealed a dimension of 300 nm, surpassing the dimensions of drug-loaded liposomes preserved at 4 °C, which measured 260 nm, following a 60-day timeframe. Also, the EE% of CIS released from the liposomal formulation at 4 °C and 25 °C after 60 days was 63.29 % and 55.37 %, respectively. For DOX, the EE% was 70.37 % at 25 °C and 76.69 % at 4 °C (Figur 5C). The results show that the percentage of entrapment efficiency for DOX was higher than that of CIS. The results clearly show that the percentage of entrapment efficiency for DOX exceeded that of CIS. This variance can be attributed to the electrostatic interactions between DOX and liposomes and the formation of amide and hydrogen bonds with liposomes, in contrast to CIS.

PDI increased with storage time due to the drug leakage out of the liposomal formulations (Fig. 5B).

Table 4
The kinetic release models and the parameters obtained for optimum liposomal formulation.

Kinetic Model		Zero-Order	First-Order	Higuchi	Korsmeyer-Peppas	
		$C_t = C_0 + K_0 t$	$LogC = LogC0 + K_t/2.303$	$Q = K_H \sqrt{t}$	$M_t/M_\infty = K_t.t^n$	
		r^2	r^2	r^2	r^2	n[a]
DOX (aq)		0.4530	0.9167	0.6250	0.744	0.463
CIS (aq)		0.4565	0.8475	0.6284	0.772	0.453
DOX + CIS@Liposome-7.4	**DOX**	0.7435	0.8242	0.8895	0.921	0.492
	CIS	0.7552	0.8154	0.8974	0.924	0.527
DOX + CIS@Liposome-5.4	**DOX**	0.8076	0.9334	0.9344	0.953	0.475
	CIS	0.7640	0.8452	0.9041	0.9229	0.484

[a] Diffusion or release exponent.

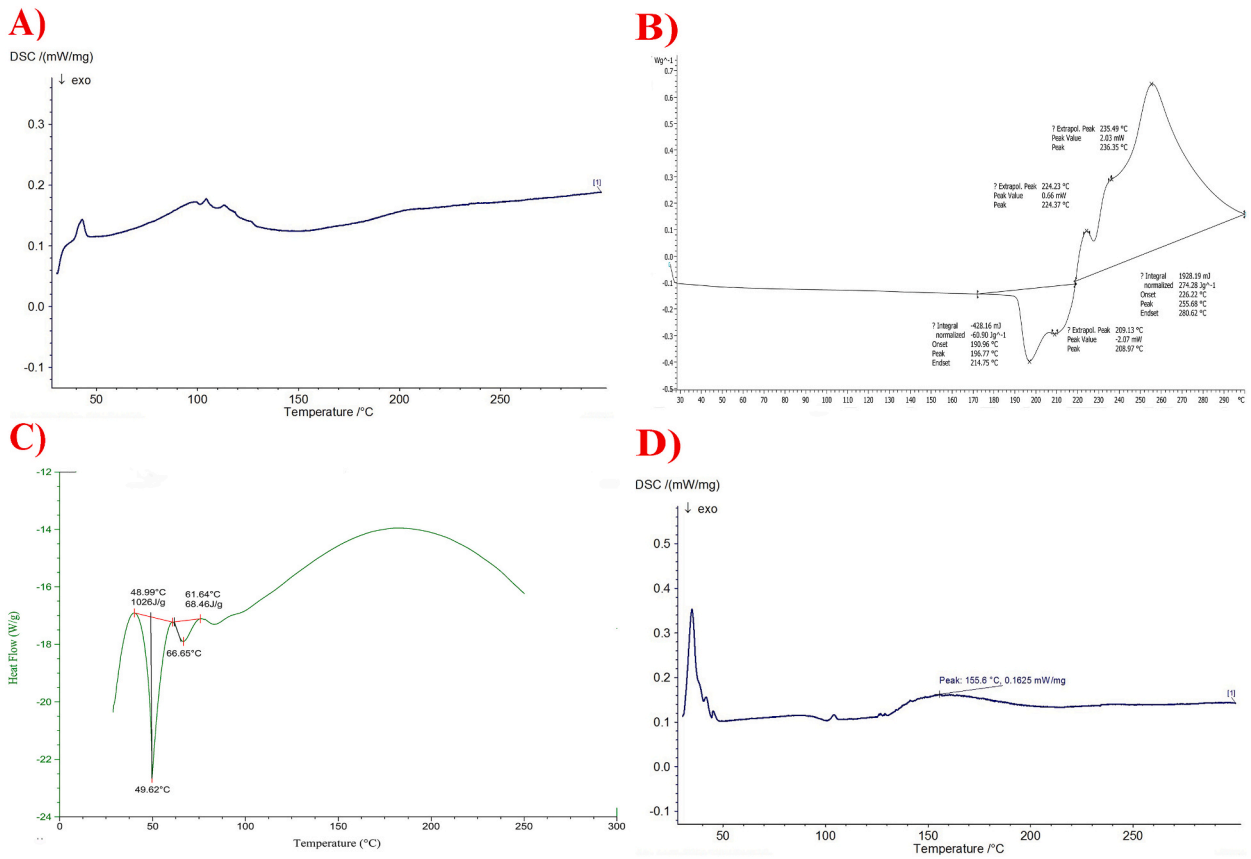

Fig. 4. Dsc of (A) Liposome, (B) DOX, (C) CIS, (D) Lipo (CIS + DOX).

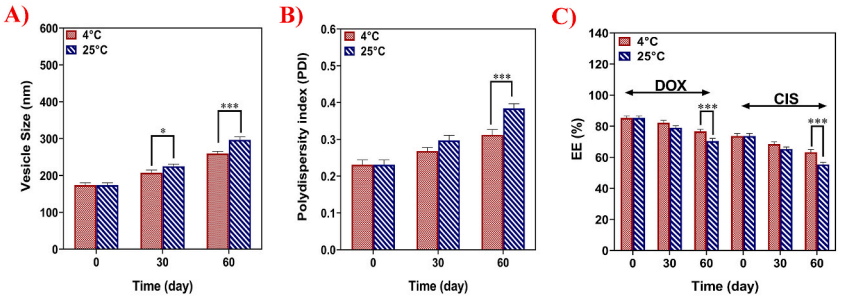

Fig. 5. The physical stability of Lipo (CIS + DOX) at 4 and 25 °C after 60 days (Mean ± SD, n = 3).

3.7. Cytotoxicity studies

The field of biomedicine is advancing at an accelerated pace compared to the past. Consequently, a category of entities known as nano-scale compounds, encompassing organic and inorganic nanoparticles, has emerged within biomedical applications, displaying diverse configurations, surface attributes, and dimensions [63]. Liposomes, which are hydrophilic, spherical bilayer vesicles composed of phospholipids, have gained prominence. Their capability to encapsulate hydrophilic and lipophilic drugs makes them among the most preferred nano-carriers. Noteworthy features of liposomes encompass their cell-membrane resemblance, safeguarding of active groups, minimal immunogenicity, safety, biocompatibility, and efficacy [64]. This study underscores the excellent biocompatibility of the Lipo (CIS + DOX) formulation with the HFF cell line. Furthermore, it is noteworthy that empty liposomes demonstrated no toxicity toward the HFF cell line (Fig. 6A).

The analysis of cytotoxic effects on A2780 cells, using varying concentrations of empty liposomes (Lipo), CIS, DOX, CIS + DOX, and Lipo (CIS + DOX), was conducted over 24 and 48 h (Fig. 6B and C). All samples' cell viability significantly declined ($P < 0.001$) in correlation with increasing concentrations. As depicted in Fig. 6D, the IC_{50} values for the CIS + DOX formulation demonstrated a

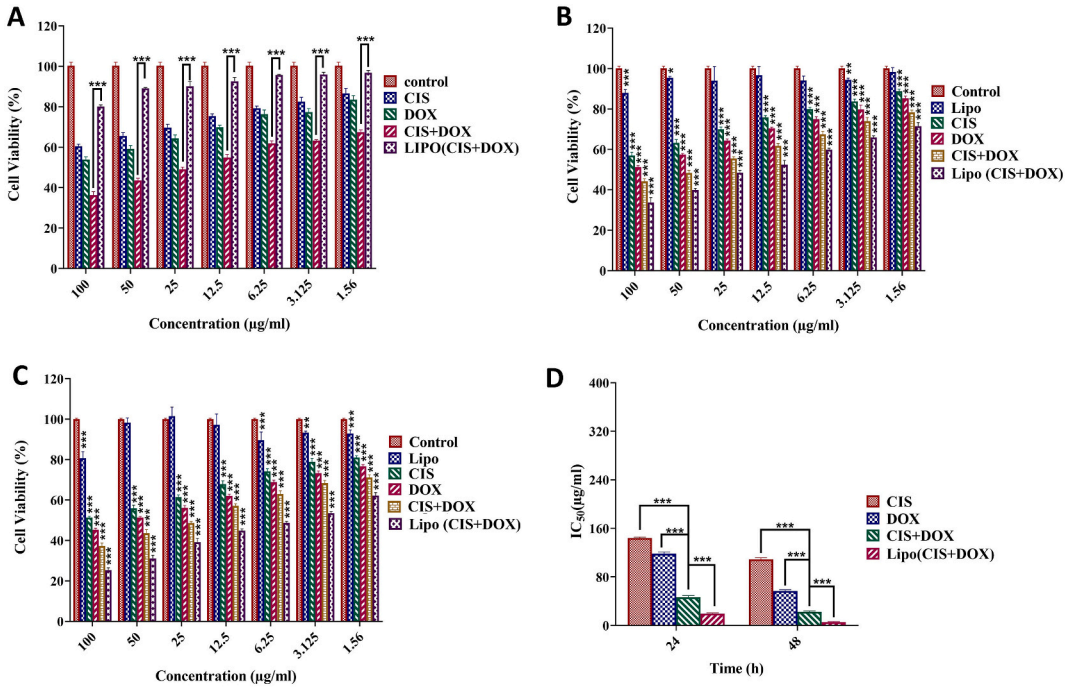

Fig. 6. Cytotoxicity effects of unloaded liposomes (Lipo), free CIS, free DOX, CIS + DOX, and Lipo (CIS + DOX) in 24 h on HFF cell line (A); Cytotoxicity effects of unloaded liposomes (Lipo), free CIS, free DOX, CIS + DOX, and Lipo (CIS + DOX) in 24 h (B), and 48 h (C) against A2780 cancer cells; Comparison between IC_{50} of all samples on A2780 cells in 24 and 48 h (D); Data represent means ± standard deviations (n = 3). For all charts, ***: $P < 0.001$; **: $P < 0.01$; *: $P < 0.05$.

notable reduction ($P < 0.001$) compared to free CIS and DOX after 24 and 48 h. Moreover, the reduction in IC_{50} for Lipo (CIS + DOX) surpassed that of CIS + DOX. Additionally, considerable reductions ($P < 0.001$) in IC_{50} values were evident for CIS, DOX, CIS + DOX, and Lipo (CIS + DOX) after 48 h when compared to the 24-h treatment (Fig. 6D).

Given the heightened efficacy of dual chemotherapy agents over single agents, combining chemotherapy drugs has become integral to chemotherapeutic strategies [65]. This approach mitigates drug-related toxic side effects and enhances treatment effectiveness by optimizing the concentrations required to elicit desired outcomes [66]. The amalgamation of CIS and DOX in an anticancer drug system holds promise, as it facilitates lower drug dosages and mitigates cardiotoxicity concerns [67].

The efficacy of many chemotherapeutic agents may be compromised due to rapid metabolism, adverse reactions, and the emergence of drug resistance. Nano-carriers, such as liposomes, have been harnessed to enhance the therapeutic efficacy of several chemotherapeutic agents, circumventing these limitations. Liposomes leverage the enhanced permeability and retention (EPR) mechanism, enabling passive targeting and accumulation in tumors and inflammatory sites, along with improved pharmacokinetic attributes of the enclosed medication. They concurrently reduce the systemic toxicity of the free drug. Additionally, liposomes enhance drug solubility and provide a controlled, sustained release of encapsulated molecules.

Nevertheless, it is imperative to acknowledge that nanoparticles, particularly liposomes, still entail some toxicity risk and lack precise targeting and distribution, notwithstanding their efficacy in treating diverse malignancies [68]. The augmentation of anti-tumor effects and the mitigation of systemic toxicity via nano liposomal formulations assume significance through sustained drug release, in contrast to free drugs [69]. Our findings indicate that the controlled release of nano liposomal drugs exhibited substantial toxicity against A2780 cancer cells over 24 and 48 h while exerting minimal effects on the HFF healthy cell line. The biocompatibility of the Lipo (CIS + DOX) formulation with the HFF cell line was pronounced. Cytotoxicity data for Lipo (CIS + DOX) suggests that CIS and DOX release within cells govern cytotoxicity rather than being governed by components of the liposomal formulation [70].

According to the results obtained, CIS and DOX liposomal systems exhibit heightened cytotoxicity compared to single-loaded liposomal formulations presented in prior studies. Furthermore, the IC_{50} values for Lipo (CIS + DOX) were notably lower than those for CIS-Lipo and DOX-Lipo [71,72]. Additionally, the IC_{50} values for Lipo (CIS + DOX) against A2780 cancer cells after 48 h were 6.22 µg/mL, demonstrating a reduction compared to (CIS + DOX) liposomal systems employed against other cancer cell types [73,74]. The synergistic effect of Lipo (CIS + DOX) cytotoxicity against A2780 cancer cells surpassed that of other single or dual drug-loaded liposomes [75,76]. Maswadeh et al. reported that Doxorubicin loaded into thermosensitive liposomes exhibited a 20-fold reduction in IC_{50} at 42 °C compared to 37 °C. The findings also demonstrated a 35-fold and 12-fold decrease in IC_{50} for cisplatin thermosensitive liposomes at 42 °C, relative to free cisplatin and cisplatin-thermosensitive liposomes at any temperature, respectively [77].

3.8. Detection of apoptosis and necrosis

In order to assess the rate of cellular apoptosis, the double staining technique employing FITC-Annexin V and propidium iodide (PI) was employed to incubate the cancer cells. According to the data presented in Fig. 7, the apoptosis rate for the A2780 cell line was found to be 65.6 ± 1.13 % for CIS, 65.15 ± 1.48 % for DOX, 69.8 ± 0.85 % for CIS + DOX, 90.15 ± 0.78 % for Lipo (CIS + DOX), and 2.10 ± 0.34 % for unloaded liposomes (Lipo). All formulations exhibited a significant increase in apoptosis rates compared to the control group ($P < 0.001$). Moreover, the results indicated a notable increase in apoptosis rates when combining CIS + DOX instead of using CIS or DOX individually ($P < 0.05$). Furthermore, the apoptotic rate of A2780 cells was significantly higher when treated with Lipo (CIS + DOX) compared to CIS + DOX alone ($P < 0.001$). The combination of CIS and DOX demonstrated synergistic effects, enhancing their efficacy in eradicating ovarian cancer cells due to their mutually reinforcing inhibitory impact. Additionally, the encapsulation of potent drugs within nano-carriers considerably amplifies their effectiveness in inducing apoptosis in ovarian cancer cells [78].

Furthermore, DOX, an anthracycline antibiotic, can impede DNA remodeling through intercalation within DNA nucleotides and inhibition of topoisomerase II activity. CIS, on the other hand, acts as a potent DNA chelating agent that forms DNA adducts. CIS induces apoptosis in cancer cells by creating covalent bonds with DNA purine bases. Consequently, it hinders cellular transcription and replication processes, thus disrupting cellular repair mechanisms [79,80].

The Lipo (CIS + DOX) formulation notably augments the apoptotic rate in cancer cells compared to other formulations. Liposomes initiate apoptosis by activating procaspase outside the cell, leading to swift cascade cleavage and a subsequent elevation in death signals [81]. In the study conducted by Maswadeh et al. treatment with doxorubicin-loaded thermosensitive liposomes resulted in over 25 % apoptotic cells in tumor cells, as determined by flow cytometry. The result underscores the superior efficacy of thermosensitive liposomal treatment loaded with doxorubicin and cisplatin under hyperthermic conditions [77]. Similarly, a study on liposome-coated nano-doxorubicin demonstrated a more significant apoptotic influence on oral squamous cell carcinoma CAL-27 cells than DOX alone. These findings were corroborated by elevated caspase-3 expression and reduced C-Myc expression [82].

In another investigation, Singh et al. demonstrated that liposomes carrying a combination of DOX and celecoxib exhibited significant anticancer effects, yielding a cancer cell viability reduction of over 99 %, even at lower concentrations than free drugs. This effect might be attributed to synergistic inhibition of the AKT and COX-2 pathways, ultimately leading to cellular apoptosis [83]. Conversely, contrasting the study by Novais et al. an evaluation of cell cycle and death pathways revealed that liposomes co-encapsulating doxorubicin and a glucoevatromonoside derivative prompted apoptosis and necrosis in breast cancer cell lines [84]. Strikingly, in contrast to Novais et al. study, our necrotic results showed the significant reduction in the necrotic rate in ovarian cells treated with Lipo (CIS + DOX) compared to (CIS + DOX) or single drugs, which could be the new findings in the field of cancer therapy.

3.9. Cell cycle arrest analysis

Cell cycle alterations were evaluated to elucidate the growth-inhibitory effect of liposomes further. Flow cytometry was employed to investigate the impact of different formulations, including empty liposomes (Lipo), free CIS, free DOX, CIS + DOX, and liposomes encapsulating CIS + DOX, on the cell cycle progression of cancerous cells (Fig. 8). Research indicates that the CIS + DOX and liposomal CIS + DOX formulations induce cell cycle arrest in A2780 cells during the sub-G1 phase (29.72 ± 0.18 % for liposomal CIS + DOX and

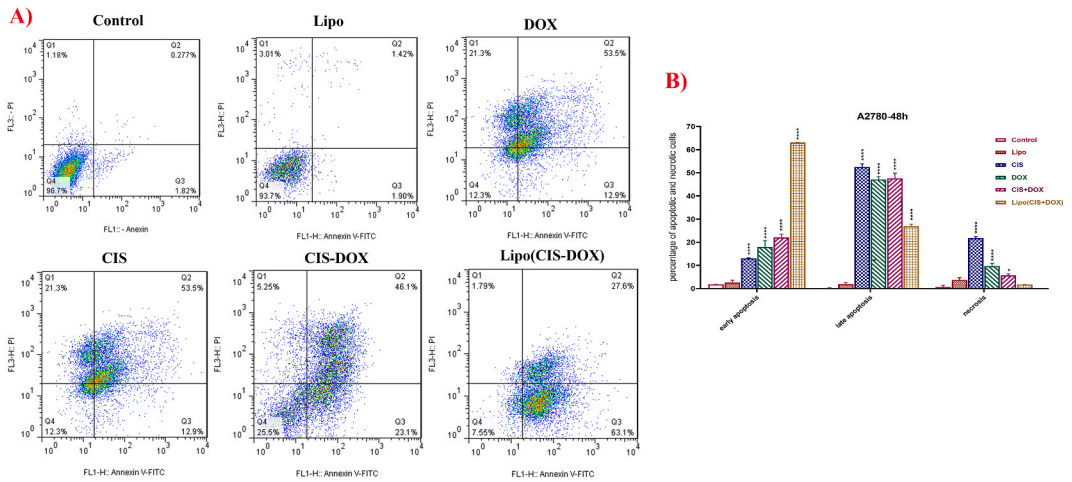

Fig. 7. Flow cytometric plots for evaluating apoptosis of A2780 cells after treatment with IC_{50} concentration of unloaded liposomes (Lipo), free CIS, free DOX, CIS + DOX, and Lipo (CIS + DOX) formulations. The upper left square (Q1) shows the percentage of necrotic cells and the upper right square (Q2) exhibits the percentage of late apoptotic cells, (Q3) exhibits the percentage of early apoptotic cells, and (Q4) shows the percentage of live cells (A). Comparison of the apoptosis induction in the A2780 cancer cells after the treatment with the different formulations (B). Data presented means standard deviation (n = 3). For all graphs, ****: P < 0.0001; *: P < 0.05.

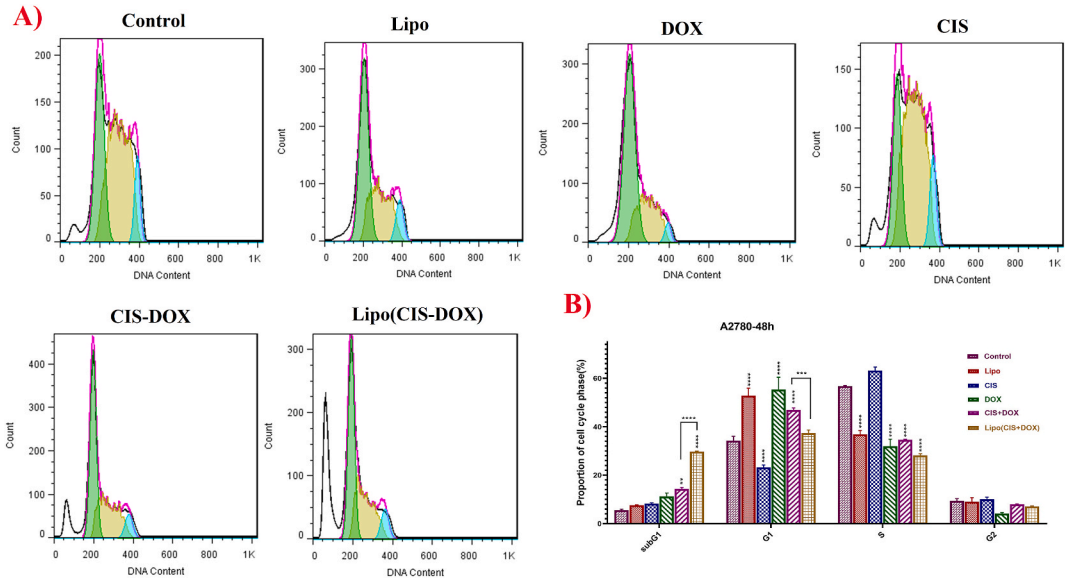

Fig. 8. Flow cytometry plots of cell cycle arrest in A2780 cancer cells following treatment with IC_{50} concentration of unloaded liposome (Lipo), free CIS, free DOX, CIS + DOX, and Lipo (CIS + DOX) formulation (A). Cell cycle distribution analysis for A2780 cancer cells after treatment with different formulations (B). Data presented means standard deviation (n = 3). For all graphs, ****: $P < 0.0001$; **: $P < 0.01$.

14.37 ± 0.56 % for CIS + DOX). As depicted in Fig. 8, the cell population of the samples exhibited significant enhancement compared to the controls following incubation with IC_{50} concentrations. The combination of CIS and DOX acts on multiple targets during distinct cell cycle phases, allowing for a reduction in the required dosage when administered together. DOX arrests the cell cycle at G2/M, while CIS inhibits the cell cycle at the G2 phase [85,86]. According to a study by Novais et al. it was confirmed that liposomes co-encapsulating doxorubicin and a glucoevatromonoside derivative could arrest the cell cycle in the G2/M phase, leading to apoptosis in breast cancer cell lines [84].

4. Conclusion

Liposome-based nano-carriers were prepared using a thin-film layer to simultaneously deliver CIS and DOX, aiming to enhance the chemotherapeutic effect on ovarian cancer. The results demonstrate that liposomal CIS + DOX (Lipo) exhibits higher stability in physiological pH compared to free drugs. At the cellular level, liposomal CIS + DOX (Lipo) significantly reduces the IC_{50} concentrations against A2780 and HFF cell lines, outperforming the free drug combination, individual free drugs, and empty liposomal formulation. Furthermore, liposomal CIS + DOX (Lipo) induces substantial apoptosis in the tested ovarian cancer cells. Consequently, these liposomal nano-carriers loaded with dual drugs have the potential to act as synergistic compounds for the treatment of ovarian cancer. Further in vivo experiments can elucidate the potential of the liposomal formulation of cisplatin and doxorubicin to be used as a drug for cancer treatment.

Funding

There is no funding.

Authors' contribution

Mahdi Bahrami Parsa: Conceived and designed the experiments; Contributed reagents, materials; Performed the experiments; Analyzed and interpreted the data; Wrote the paper. Farzaneh Tafvizi: Conceived and designed the experiments; Contributed reagents, materials, analysis tools or data; Analyzed and interpreted the data; Wrote the paper. Vahid Chaleshi: Contributed reagents, materials, analysis tools or data.

Informed consent

All authors consent to the publication of this study.

Data availability

The datasets used and/or analyzed during the current study are available from the corresponding author on reasonable request.

CRediT authorship contribution statement

Mahdi Bahrami Parsa: Data curation, Formal analysis, Methodology, Writing – original draft. **Farzaneh Tafvizi:** Data curation, Methodology, Project administration, Supervision, Writing – original draft, Writing – review & editing. **Vahid Chaleshi:** Formal analysis, Investigation, Methodology. **Mostafa Ebadi:** Formal analysis, Methodology, Writing – review & editing.

Declaration of competing interest

The authors declare that they have no known competing financial interests or personal relationships that could have appeared to influence the work reported in this paper.

Acknowledgements

The authors would like to acknowledge the laboratory of Islamic Azad University.

Appendix A. Supplementary data

Supplementary data to this article can be found online at https://doi.org/10.1016/j.heliyon.2023.e20657.

References

[1] D. Holmes, Ovarian cancer: beyond resistance, Nature 527 (7579) (2015). S217-S217.
[2] V.W. Chen, B. Ruiz, J.L. Killeen, T.R. Coté, X.C. Wu, C.N. Correa, H.L. Howe, Pathology and classification of ovarian tumors, Cancer, Interdisciplinary International Journal of the American Cancer Society 97 (S10) (2003) 2631–2642.
[3] G.D. Aletti, M.M. Gallenberg, W.A. Cliby, A. Jatoi, L.C. Hartmann, Current Management Strategies for Ovarian Cancer, Mayo Clinic Proceedings, Elsevier, 2007, pp. 751–770.
[4] G. Di Lorenzo, G. Ricci, G.M. Severini, F. Romano, S. Biffi, Imaging and therapy of ovarian cancer: clinical application of nanoparticles and future perspectives, Theranostics 8 (16) (2018) 4279.
[5] A. Chandra, C. Pius, M. Nabeel, M. Nair, J.K. Vishwanatha, S. Ahmad, R. Basha, Ovarian cancer: current status and strategies for improving therapeutic outcomes, Cancer Med. 8 (16) (2019) 7018–7031.
[6] A. Arabzadeh, T. Mortezazadeh, T. Aryafar, E. Gharepapagh, M. Majdaeen, B. Farhood, Therapeutic potentials of resveratrol in combination with radiotherapy and chemotherapy during glioblastoma treatment: a mechanistic review, Cancer Cell Int. 21 (1) (2021) 1–15.
[7] T.L. Jackson, H.M. Byrne, A mathematical model to study the effects of drug resistance and vasculature on the response of solid tumors to chemotherapy, Math. Biosci. 164 (1) (2000) 17–38.
[8] Y. Hussain, L. Islam, H. Khan, R. Filosa, M. Aschner, S. Javed, Curcumin–cisplatin chemotherapy: a novel strategy in promoting chemotherapy efficacy and reducing side effects, Phytother Res. 35 (12) (2021) 6514–6529.
[9] Q. Hu, W. Sun, C. Wang, Z. Gu, Recent advances of cocktail chemotherapy by combination drug delivery systems, Adv. Drug Deliv. Rev. 98 (2016) 19–34.
[10] C.-M.J. Hu, S. Aryal, L. Zhang, Nanoparticle-assisted combination therapies for effective cancer treatment, Ther. Deliv. 1 (2) (2010) 323–334.
[11] S. Dasari, P.B. Tchounwou, Cisplatin in cancer therapy: molecular mechanisms of action, Eur. J. Pharmacol. 740 (2014) 364–378.
[12] S. Ghosh, Cisplatin: the first metal-based anticancer drug, Bioorg. Chem. 88 (2019), 102925.
[13] L. Astolfi, S. Ghiselli, V. Guaran, M. Chicca, E. Simoni, E. Olivetto, G. Lelli, A. Martini, Correlation of adverse effects of cisplatin administration in patients affected by solid tumors: a retrospective evaluation, Oncol. Rep. 29 (4) (2013) 1285–1292.
[14] S. Barui, S. Saha, G. Mondal, S. Haseena, A. Chaudhuri, Simultaneous delivery of Doxorubicin and curcumin encapsulated in liposomes of pegylated RGDK-lipopeptide to tumor vasculature, Biomaterials 35 (5) (2014) 1643–1656.
[15] K.B. Wallace, Doxorubicin-induced cardiac mitochondrionopathy, Pharmacol. Toxicol. 93 (3) (2003) 105–115.
[16] J. Sastry, S.J. Kellie, Severe neurotoxicity, ototoxicity and nephrotoxicity following high-dose Cisplatin and amifostine, Pediatr. Hematol. Oncol. 22 (5) (2005) 441–445.
[17] E.C. Gryparis, M. Hatziapostolou, E. Papadimitriou, K. Avgoustakis, Anticancer activity of cisplatin-loaded PLGA-mPEG nanoparticles on LNCaP prostate cancer cells, Eur. J. Pharm. Biopharm. 67 (1) (2007) 1–8.
[18] J. Fujiyama, Y. Nakase, K. Osaki, C. Sakakura, H. Yamagishi, A. Hagiwara, Cisplatin incorporated in microspheres: development and fundamental studies for its clinical application, J. Contr. Release 89 (3) (2003) 397–408.
[19] X. Zhang, W. Zong, J. Wang, M. Dong, W. Cheng, T. Sun, X. Han, Multicompartmentalized vesosomes containing DOX loaded liposomes and 5FU loaded liposomes for synergistic tumor treatment, New J. Chem. 43 (12) (2019) 4895–4899.
[20] C. Li, H. Guan, Z. Li, F. Wang, J. Wu, B. Zhang, Study on different particle sizes of DOX-loaded mixed micelles for cancer therapy, Colloids Surf. B Biointerfaces 196 (2020), 111303.
[21] P. Anand, A.B. Kunnumakkara, R.A. Newman, B.B. Aggarwal, Bioavailability of curcumin: problems and promises, Mol. Pharm. 4 (6) (2007) 807–818.
[22] A. Sanchez-Munoz, E. Perez-Ruiz, N. Ribelles, A. Marquez, E. Alba, Maintenance treatment in metastatic breast cancer, Expet Rev. Anticancer Ther. 8 (12) (2008) 1907–1912.
[23] S. Biju, S. Talegaonkar, P. Mishra, R. Khar, Vesicular systems: an overview, Indian J. Pharmaceut. Sci. 68 (2) (2006).
[24] C. Marianecci, S. Petralito, F. Rinaldi, P.N. Hanieh, M. Carafa, Some recent advances on liposomal and niosomal vesicular carriers, J. Drug Deliv. Sci. Technol. 32 (2016) 256–269.
[25] A. Akbarzadeh, R. Rezaei-Sadabady, S. Davaran, S.W. Joo, N. Zarghami, Y. Hanifehpour, M. Samiei, M. Kouhi, K. Nejati-Koshki, Liposome: classification, preparation, and applications, Nanoscale Res. Lett. 8 (1) (2013) 1–9.
[26] R. Mara Mainardes, M. Cristina Cocenza Urban, P. Oliveira Cinto, M. Vinicius Chaud, R. Cesar Evangelista, M. Palmira Daflon Gremiao, Liposomes and micro/nanoparticles as colloidal carriers for nasal drug delivery, Curr. Drug Deliv. 3 (3) (2006) 275–285.

[27] A. Dhiman, A. Nanda, S. Ahmad, Novel herbal drug delivery system (NHDDS): the need of the hour, International Conference on Environment, Chemistry and Biology (2012) 171–175.
[28] L. Mohammed, H. Nourddine, D. Abdelali, R. Hamid, Chitosan-covered liposomes as a promising drug transporter: nano-scale investigations, RSC Adv. 11 (3) (2021) 1503–1516.
[29] A. Carvalho Júnior, F. Vieira, V. De Melo, M. Lopes, J. Silveira, G. Ramaldes, A. Garnier-Suillerot, E. Pereira-Maia, M. De Oliveira, Preparation and cytotoxicity of cisplatin-containing liposomes, Braz. J. Med. Biol. Res. 40 (8) (2007) 1149–1157.
[30] C. Zhang, C. Xu, X. Gao, Q. Yao, Platinum-based drugs for cancer therapy and anti-tumor strategies, Theranostics 12 (5) (2022) 2115.
[31] G.F. Fleming, V.L. Brunetto, D. Cella, K.Y. Look, G.C. Reid, A.R. Munkarah, R. Kline, R.A. Burger, A. Goodman, R.T. Burks, Phase III trial of Doxorubicin plus Cisplatin with or without paclitaxel plus filgrastim in advanced endometrial carcinoma: a Gynecologic Oncology Group Study, J. Clin. Oncol. 22 (11) (2004) 2159–2166.
[32] H.M. Katzenstein, M.H. Malogolowkin, M.D. Krailo, J. Piao, A.J. Towbin, M.B. McCarville, G.M. Tiao, S.P. Dunn, M.R. Langham, E.D. McGahren, Doxorubicin in combination with Cisplatin, 5-flourouracil, and vincristine is feasible and effective in unresectable hepatoblastoma: a Children's Oncology Group study, Cancer 128 (5) (2022) 1057–1065.
[33] H. Wu, H. Jin, C. Wang, Z. Zhang, H. Ruan, L. Sun, C. Yang, Y. Li, W. Qin, C. Wang, Synergistic cisplatin/doxorubicin combination chemotherapy for multidrug-resistant cancer via polymeric nanogels targeting delivery, ACS applied materials & interfaces 9 (11) (2017) 9426–9436.
[34] X.-L. Guo, X.-X. Kang, Y.-Q. Wang, X.-J. Zhang, C.-J. Li, Y. Liu, L.-B. Du, Co-delivery of Cisplatin and Doxorubicin by covalently conjugating with polyamidoamine dendrimer for enhanced synergistic cancer therapy, Acta Biomater. 84 (2019) 367–377.
[35] J.T. Thigpen, M.F. Brady, H.D. Homesley, J. Malfetano, B. DuBeshter, R.A. Burger, S. Liao, Phase III trial of Doxorubicin with or without Cisplatin in advanced endometrial carcinoma: a gynecologic oncology group study, J. Clin. Oncol. 22 (19) (2004) 3902–3908.
[36] Q. Chen, Y. Yang, X. Lin, W. Ma, G. Chen, W. Li, X. Wang, Z. Yu, Platinum (iv) prodrugs with long lipid chains for drug delivery and overcoming cisplatin resistance, Chemical communications 54 (42) (2018) 5369–5372.
[37] S.Z. Vahed, R. Salehi, S. Davaran, S. Sharifi, Liposome-based drug co-delivery systems in cancer cells, Mater. Sci. Eng. C 71 (2017) 1327–1341.
[38] R.-J. Ju, F. Zeng, L. Liu, L.-M. Mu, H.-J. Xie, Y. Zhao, Y. Yan, J.-S. Wu, Y.-J. Hu, W.-L. Lu, Destruction of vasculogenic mimicry channels by targeting epirubicin plus celecoxib liposomes in treatment of brain glioma, International Journal of nanomedicine (2016) 1131–1146.
[39] M.-G. Sun, J.-F. Shi, X.-Y. Li, Y. Zhao, R.-J. Ju, L.-M. Mu, Y. Yan, X.-T. Li, F. Zeng, W.-L. Lu, Targeting epirubicin plus quinacrine liposomes modified with DSPE-PEG2000-C (RGDfK) conjugate for eliminating invasive breast cancer, J. Biomed. Nanotechnol. 11 (8) (2015) 1339–1353.
[40] F. Zeng, R.-J. Ju, L. Liu, H.-J. Xie, L.-M. Mu, Y. Zhao, Y. Yan, Y.-J. Hu, J.-S. Wu, W.-L. Lu, Application of functional vincristine plus dasatinib liposomes to deletion of vasculogenic mimicry channels in triple-negative breast cancer, Oncotarget 6 (34) (2015), 36625.
[41] H.M. Maswadeh, A. Khan, M.S. Alorainy, N.A. Al-Wabel, C. Demetzos, Concomitant delivery of Doxorubicin and Cisplatin through liposome-based thermosensitive nanoparticles: perspective in the treatment of cancer in animal models, Am. J. Cancer Res. 13 (2) (2023) 379.
[42] H. Zhang, Thin-film Hydration Followed by Extrusion Method for Liposome Preparation, Liposomes, Methods and protocols, 2017, pp. 17–22.
[43] S. Dash, P.N. Murthy, L. Nath, P. Chowdhury, Kinetic modeling on drug release from controlled drug delivery systems, Acta Pol. Pharm. 67 (3) (2010) 217–223.
[44] S.R.M. Moghddam, A. Ahad, M. Aqil, S.S. Imam, Y. Sultana, Formulation and optimization of niosomes for topical diacerein delivery using 3-factor, 3-level Box-Behnken design for the management of psoriasis, Mater. Sci. Eng. C 69 (2016) 789–797.
[45] Z. Wang, X. He, Dynamics of vesicle formation from lipid droplets: mechanism and controllability, The Journal of chemical physics 130 (9) (2009), 094905.
[46] D. Mohanty, M.J. Rani, M.A. Haque, V. Bakshi, M.A. Jahangir, S.S. Imam, S.J. Gilani, Preparation and evaluation of transdermal naproxen niosomes: formulation optimization to preclinical anti-inflammatory assessment on murine model, J. Liposome Res. 30 (4) (2020) 377–387.
[47] S. Taymouri, J. Varshosaz, Effect of different types of surfactants on the physical properties and stability of carvedilol nano-niosomes, Adv. Biomed. Res. 5 (2016).
[48] S.G. Amin, D.A. Shah, R.H. Dave, Formulation and evaluation of liposomes of fenofibrate prepared by thin film hydration technique, Int. J. Pharm. Sci. Res 9 (9) (2018) 3621–3637.
[49] K. Ruckmani, V. Sankar, Formulation and optimization of zidovudine niosomes, AAPS PharmSciTech 11 (3) (2010) 1119–1127.
[50] L. Lopes, M. Scarpa, G. Silva, D. Rodrigues, C. Santilli, A.G.d. Oliveira, Studies on the encapsulation of diclofenac in small unilamellar liposomes of soya phosphatidylcholine, Colloids Surf., B: bio interfaces 39 (4) (2004) 151–158.
[51] R.M. Zaki, A.A. Ali, S.F. El Menshawe, A.A. Bary, Formulation and in vitro evaluation of diacerein loaded niosomes, Int J Pharm Pharm Sci 6 (Suppl 2) (2014) 515–521.
[52] A.A. Abdelbary, M.H. AbouGhaly, Design and optimization of topical methotrexate loaded niosomes for enhanced management of psoriasis: application of Box–Behnken design, in-vitro evaluation and in-vivo skin deposition study, International journal of pharmaceutics 485 (1–2) (2015) 235–243.
[53] Y. Li, L. Yang, Driving forces for drug loading in drug carriers, J. Microencapsul. 32 (3) (2015) 255–272.
[54] J.S. Suk, Q. Xu, N. Kim, J. Hanes, L.M. Ensign, PEGylation as a strategy for improving nanoparticle-based drug and gene delivery, Adv. Drug Deliv. Rev. 99 (2016) 28–51.
[55] J. Tian, X. Pang, K. Yu, L. Liu, J. Zhou, Preparation, characterization and in vivo distribution of solid lipid nanoparticles loaded with Cisplatin, Die Pharmazie-An International Journal of Pharmaceutical Sciences 63 (8) (2008) 593–597.
[56] M. Liu, X. Zhang, B. Yang, F. Deng, J. Ji, Y. Yang, Z. Huang, X. Zhang, Y. Wei, Luminescence tunable fluorescent organic nanoparticles from polyethyleneimine and maltose: facile preparation and bioimaging applications, RSC advances 4 (43) (2014) 22294–22298.
[57] A. Mirzaie, N. Peirovi, I. Akbarzadeh, M. Moghtaderi, F. Heidari, F.E. Yeganeh, H. Noorbazargan, S. Mirzazadeh, R. Bakhtiari, Preparation and optimization of ciprofloxacin encapsulated niosomes: a new approach for enhanced antibacterial activity, biofilm inhibition and reduced antibiotic resistance in ciprofloxacin-resistant methicillin-resistance Staphylococcus aureus, Bioorg. Chem. 103 (2020), 104231.
[58] S. Rayamajhi, J. Marchitto, T.D.T. Nguyen, R. Marasini, C. Celia, S. Aryal, pH-responsive cationic liposome for endosomal escape mediated drug delivery, Colloids Surf. B Biointerfaces 188 (2020), 110804.
[59] D.R. Nogueira, L. Tavano, M. Mitjans, L. Pérez, M.R. Infante, M.P. Vinardell, In vitro antitumor activity of methotrexate via pH-sensitive chitosan nanoparticles, Biomaterials 34 (11) (2013) 2758–2772.
[60] M. Khafaji, M. Zamani, M.J.I.J.o.N. Vossoughi, Doxorubicin/cisplatin-loaded superparamagnetic nanoparticles as a stimuli-responsive co-delivery system for chemo-photothermal therapy 14 (2019) 8769.
[61] M. Shafaa, Interaction OF BISOPROLOL or ENALAPRIL with DISTEAROYL PHOSPHATIDYLCHOLINE liposomes: FTIR and DSC studies, Rom. J. Biophys. 28 (3) (2018).
[62] J.V. Natarajan, S. Chattopadhyay, M. Ang, A. Darwitan, S. Foo, M. Zhen, M. Koo, T.T. Wong, S.S. Venkatraman, Sustained release of an anti-glaucoma drug: demonstration of the efficacy of a liposomal formulation in the rabbit eye, PLoS One 6 (9) (2011), e24513.
[63] R. Khalilov, A COMPREHENSIVE review of advanced nano-BIOMATERIALS IN REGENERATIVE MEDICINE and drug delivery, Advances in Biology & Earth Sciences 8 (1) (2023).
[64] A. Eftekhari, C. Kryschi, D. Pamies, S. Gulec, E. Ahmadian, D. Janas, S. Davaran, R. Khalilov, Natural and synthetic nano vectors for cancer therapy, Nanotheranostics 7 (3) (2023) 236.
[65] I. Akbarzadeh, M. Fatemizadeh, F. Heidari, N.M. Niri, Niosomal formulation for coadministration of hydrophobic anticancer drugs into MCF-7 cancer cells, Archives of Advances in Biosciences 11 (2) (2020).
[66] A. Alemi, J. Zavar Reza, F. Haghiralsadat, H. Zarei Jaliani, M. Haghi Karamallah, S.A. Hosseini, S. Haghi Karamallah, Paclitaxel and curcumin coadministration in novel cationic PEGylated niosomal formulations exhibit enhanced synergistic anti-tumor efficacy, J. Nanobiotechnol. 16 (1) (2018) 1–20.
[67] T.H. Guthrie Jr., L.J. McElveen, E.S. Porubsky, J.D. Harmon, Cisplatin and Doxorubicin. An effective chemotherapy combination in treating advanced basal cell and squamous carcinoma of the skin, Cancer 55 (8) (1985) 1629–1632.

[68] J.J. Marin, F. Sanchez de Medina, B. Castaño, L. Bujanda, M.R. Romero, O. Martinez-Augustin, R.D. Moral-Avila, O. Briz, Chemoprevention, chemotherapy, and chemoresistance in colorectal cancer, Drug Metab. Rev. 44 (2) (2012) 148–172.
[69] A. Dwivedi, A. Mazumder, L. Du Plessis, J.L. Du Preez, R.K. Haynes, J. Du Plessis, in vitro anticancer effects of artemisone nano-vesicular formulations on melanoma cells, Nanomed. Nanotechnol. Biol. Med. 11 (8) (2015) 2041–2050.
[70] D.R. McIlwain, T. Berger, T.W. Mak, Caspase functions in cell death and disease, Cold Spring Harbor Perspect. Biol. 7 (4) (2015).
[71] M.L. Krieger, N. Eckstein, V. Schneider, M. Koch, H.-D. Royer, U. Jaehde, G. Bendas, Overcoming cisplatin resistance of ovarian cancer cells by targeted liposomes in vitro 389 (1–2) (2010) 10–17.
[72] S.K. Sriraman, G. Salzano, C. Sarisozen, V.J.E.J.o.P. Torchilin, Biopharmaceutics, Anticancer activity of doxorubicin-loaded liposomes co-modified with transferrin and folic acid 105 (2016) 40–49.
[73] W. Ma, Q. Chen, W. Xu, M. Yu, Y. Yang, B. Zou, Y.S. Zhang, J. Ding, Z.J.N.R. Yu, Self-targeting visualizable hyaluronate nanogel for synchronized intracellular release of Doxorubicin and Cisplatin in combating multidrug-resistant breast cancer 14 (3) (2021) 846–857.
[74] C. Feng, H. Zhang, J. Chen, S. Wang, Y. Xin, Y. Qu, Q. Zhang, W. Ji, F. Yamashita, M.J.I.J.o.P. Rui, Ratiometric co-encapsulation and co-delivery of Doxorubicin and paclitaxel by tumor-targeted lipodisks for combination therapy of breast cancer 560 (2019) 191–204.
[75] R.S. Faria, L.I. de Lima, R.S. Bonadio, J.P.F. Longo, M.C. Roque, J.N. de Matos Neto, S.E. Moya, M.C. de Oliveira, R.B.J.B. Azevedo, Pharmacotherapy, Liposomal paclitaxel induces apoptosis, cell death, inhibition of migration capacity and antitumoral activity in ovarian cancer 142 (2021), 112000.
[76] Y.-L. Hao, Y.-J. Deng, Y. Chen, A.-J. Hao, Y. Zhang, K.-Z.J.J.o.p. Wang, pharmacology, In-vitro cytotoxicity, -vivo biodistribution and anti-tumor effect of PEGylated liposomal topotecan 57 (10) (2005) 1279–1287.
[77] H. Maswadeh, A. Khan, M.S. Alorainy, N.A. Al-Wabel, C. Demetzos, In vitro and in vivo activity of thermosensitive liposomes loaded with Doxorubicin and Cisplatin, Drug Dev. Ind. Pharm. 48 (4) (2022) 158–168.
[78] M.S. Sharafshadeh, F. Tafvizi, P. Khodarahmi, S. Ehtesham, Preparation and physicochemical properties of Cisplatin and Doxorubicin encapsulated by niosome alginate nano-carrier for cancer therapy, Int. J. Biol. Macromol. 235 (2023), 123686.
[79] E. Tahover, Y.P. Patil, A.A.J.A.-c.d. Gabizon, Emerging delivery systems to reduce doxorubicin cardiotoxicity and improve therapeutic index: focus on liposomes 26 (3) (2015) 241–258.
[80] H. Xiao, C. Li, Y. Dai, Z. Cheng, Z. Hou, J.J.M.T. Lin, Inorganic nano-carriers for platinum drug delivery 18 (10) (2015) 554–564.
[81] D.R. McIlwain, T. Berger, T.W.J.C.S.H.P.i.B. Mak, Caspase functions in cell death and disease 7 (4) (2015).
[82] E.S. Abd El-Hamid, A.M. Gamal-Eldeen, A.M.S. Eldeen, Liposome-coated nano doxorubicin induces apoptosis on oral squamous cell carcinoma CAL-27 cells, Arch. Oral Biol. 103 (2019) 47–54.
[83] S. Singh, Liposome encapsulation of Doxorubicin and celecoxib in combination inhibits progression of human skin cancer cells, Int. J. Nanomed. 13 (sup1) (2018) 11–13.
[84] M. Novais, E. Gomes, M. Miranda, J. Silva, D. Gomes, F. Braga, R. Pádua, M. Oliveira, Liposomes co-encapsulating Doxorubicin and glucoevatromonoside derivative induce synergic cytotoxic response against breast cancer cell lines, Biomed. Pharmacother. 136 (2021), 111123.
[85] M. Viereckl, N. Alojibaily, D. Hydock, Y. Han, The Role of Creatine Supplementation in Alleviating Doxorubicin Induced Hepatotoxicity, 2020.
[86] C.M. Sorenson, M.A. Barry, A.J.J.J.o.t.N.C.I. Eastman, Analysis of events associated with cell cycle arrest at G2 phase and cell death induced by, Cisplatin 82 (9) (1990) 749–755.